Journal of Green Energy Research and Innovation

Robust Control of Load Voltage in an Islanded Wind Energy Conversion System Using Nonlinear Methods

Adel Sotoudeh, Mohammad Mahdi Rezaei, Mohammadreza Moradian

Highlight

- Using input-output controller and sliding mode simultaneously
- Load side voltage control using voltage converter
- Two-stage control of squirrel cage induction generator (SCIG)

Graphical Abstract

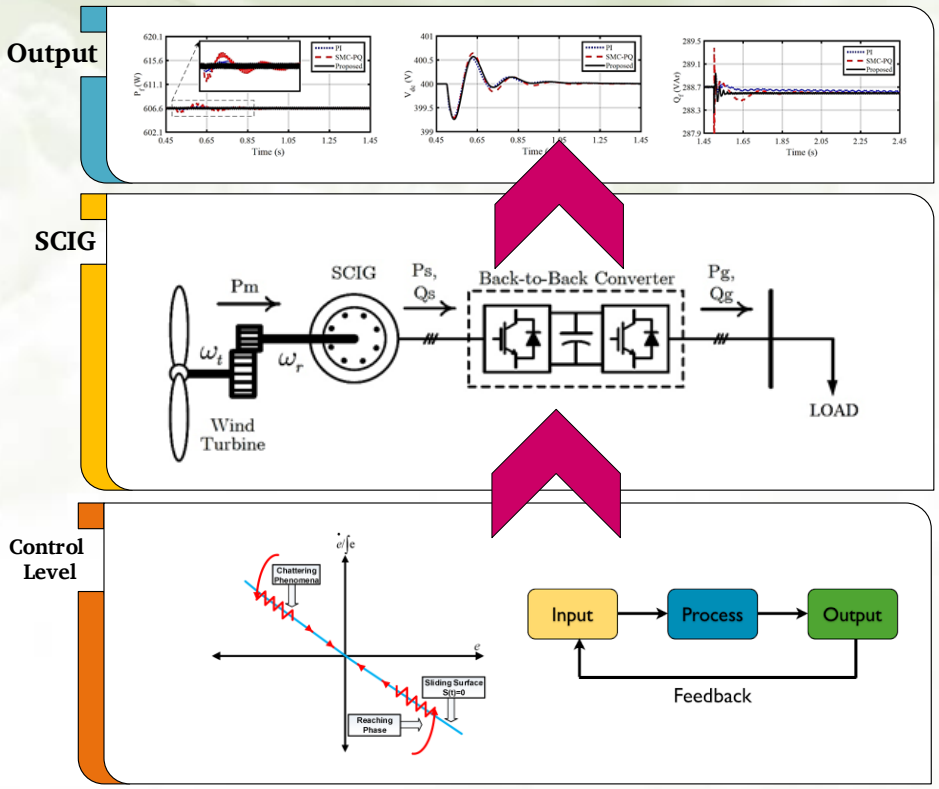

Use your device to scan and read the article online

Citation

A. Sotoudeh, M. M. Rezaei, and M. Moradian, "Robust Control of Load Voltage in an Islanded Wind Energy Conversion System Using Nonlinear Methods," *Journal of Green Energy Research and Innovation*, vol. 1, no. 4, pp. 17-34, 2024.

https://doi.org/10.61186/jgeri.1.4.17

JGERI Journal of Green Energy Research and Innovation

Online ISSN: 3041-9018

Journal of Green Energy Research and Innovation

Journal Homepage: www.jgeri.araku.ac.ir

Robust Control of Load Voltage in an Islanded Wind Energy Conversion System Using Nonlinear Methods

Adel Sotoudeh [1], Mohammad Mahdi Rezaei [1*], Mohammadreza Moradian[2]

[1] *Department of Electrical Engineering, Khomeinishahr Branch, Islamic Azad University, Khomeinishahr, Isfahan, Iran.*
[2] *Department of Electrical Engineering, Najafabad Branch, Islamic Azad University, Najafabad, Isfahan.*

* ***Corresponding Author:*** *mm.rezaei@iaukhsh.ac.ir*

ARTICLE INFO

Keywords:
Wind energy,
Induction generator,
Nonlinear control,
Feedback linearization,
Sliding mode control.

Article history:
Received: 26 April 2024;
Revised: 13 May 2024;
Accepted: 21 May 2024;

Article type:
Research Article

ABSTRACT

Renewable wind energy is a significant source of green energy supply that has gained considerable attention and development in numerous countries in recent years. These systems are utilized as islanded units in circumstances where it is not feasible to establish a connection to the network. Various structures exist for these systems, but the focus of many studies has been on wind energy conversion systems based on a squirrel cage induction machine with back-to-back converters. When operating in islanded mode, this structure necessitates specific control requirements, with the most crucial being the supplying of the desired voltage and frequency of the load. In this paper, two control structures are proposed and constructed to regulate the load voltage by controlling the load-side converter. Two control loops have been implemented in the first control structure. The inner loop utilizes the state feedback input-output method to control the voltage, while the outer loop employs the sliding mode method to control the power components. The objective is to derive the control law for the reference biaxial voltage of the load-side converter. The second proposed structure incorporates the voltage controller sliding mode control method in the inner loop and then the state feedback input-output method is employed in the outer loop to control the current components of the load-side converter, thus designing the system control input. The simulation results of both structures in MATLAB software have been compared by introducing various disturbances to assess the control systems' resilience to each other and the common proportional-integral linear control structure. In the suggested method, voltage and current variations manifest concurrently in the control structure predicated on power components.

1. Introduction

1.1. Problem Statement

The widespread utilization of fossil fuels during the 20th and 21st centuries has led to both climate change and global warming. The provision of electrical energy from renewable sources such as solar, hydro, wind, etc. as green energy has consistently been regarded as such [1]. Over the previous years, the utilization of wind energy to generate

clean power for countries has experienced significant growth. It is projected that by the end of 2030, at least 50% of the world's electricity demand will be met by this method [2]. Currently, wind energy conversion systems (WECS) are implemented in diverse structures as depicted in Figure 1 [3]. Each of these constructions can be operated either onshore or offshore. Meanwhile, the squirrel cage induction generator (SCIG), while requiring power converters with full capability, has significantly reduced maintenance costs, a smaller size, and a more affordable price compared to doubly-fed induction machines [4, 5]. The use of type F of these buildings, particularly in onshore WECS, has gained significant acceptance in recent years (Figure 2) [6].

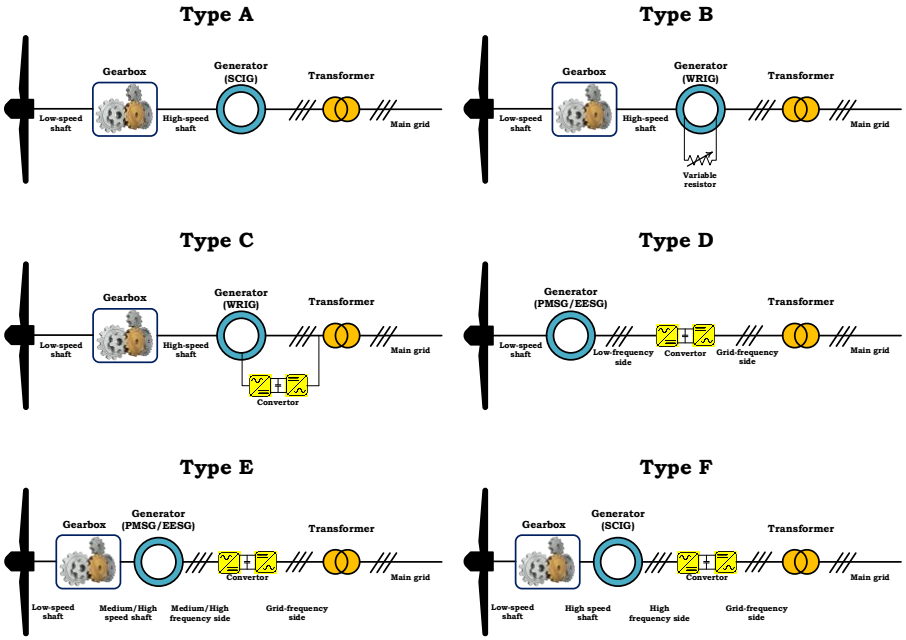

Figure 1. Types of structures used in WECS [3].

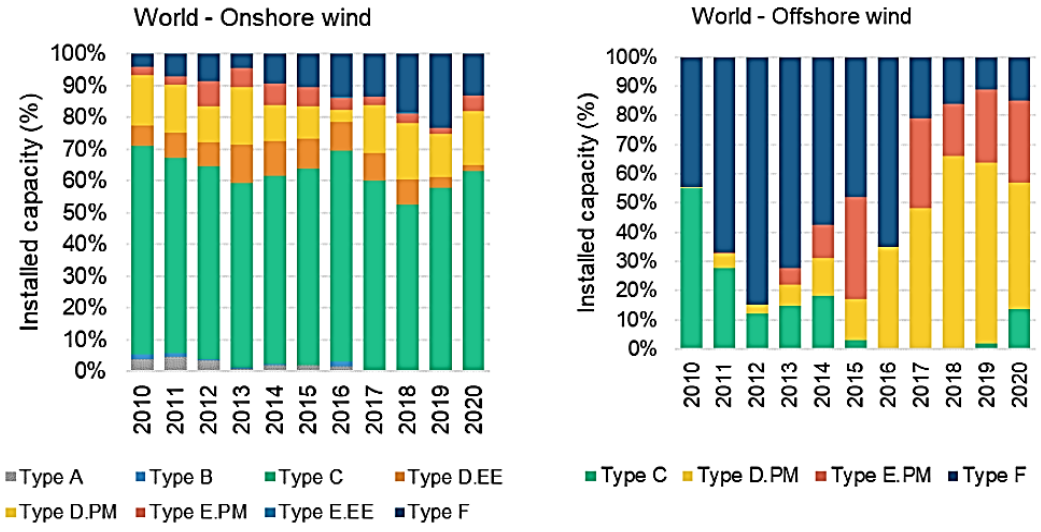

Figure 2. The rate of adoption of various wind turbine structures by the end of 2020 worldwide [6].

1.2. Literature review

The design of a control structure that aligns with the control objectives for both the machine-side converter (MSC) and network-load side converters becomes crucial in systems with back-to-back converters. These control objectives can vary in each of the modes, whether grid-connected or grid-disconnected modes. One objective that has been the focus of numerous studies in grid-connected mode is to maximize the power generated by the WECS [7] or control the power injected into the grid. The authors of this paper provided a robust control design for the mentioned objectives [8]. During islanded mode, a primary objective of the MSC is to effectively regulate the state variables of the generator to meet the energy demands of the load. Conversely, voltage and frequency controls are a highly important control target for the load side converter, as stated in [9-11]. These objectives are particularly crucial when dealing with nonlinear and unbalanced loads, as well as transient conditions [12]. In recent research, a variety of control approaches, such as linear, nonlinear, a combination of linear and nonlinear methods, and techniques based on artificial intelligence, have been employed to accomplish the stated objectives [13]. The proportional-integral (PI) linear control approach is widely utilized in research because of its simplicity. However, identifying the ideal coefficients for this method is a significant difficulty [14,15]. This method can be transformed into a nonlinear method called fractional-order PI by changing the order of its integral part. Similar to the PI method, the fractional-order PI method can be used in conjunction with other linear and nonlinear control methods. It has been observed to exhibit superior performance in transient states compared to traditional PI methods [16]. In the context of nonlinear control systems, it is worth noting the existence of sliding mode control, which can be further categorized into sub-branches such as high-order sliding mode control or fractional-order sliding mode control [17-20]. Also, in some articles, the discussion of wind turbines has been discussed only from the point of view of steady-state and efficiency improvement and cost reduction [21,22]. In addition, numerous research studies have also explored the use of input-output feedback linearization (IOFL) methods and the backward control approach [8,20]. The primary differentiation between linear and nonlinear approaches lies in their treatment of transient states. Generally, linear control methods have a straightforward design, but their ability to respond to different dynamic transient states is significantly less compared to nonlinear control systems. Moreover, linear methods often function just as regulators and exhibit a resistant behavior towards states. The lack of robust transitivity in many circumstances leads to the loss of system stability [16].

1.3. Research gaps

According to the reviewed references, there are the following research gaps in the past research:

- Most of the proposed methods have not given appropriate responses to different modes of fluctuations in the network.

- Most of the references have used methods based on the PID control method, which does not perform well against transient changes.

1.4. Innovations and research contributions

To solve the disadvantages and gaps stated in the previous part, in this article, a two-stage control method is presented, the innovations of which are as follows:

- Using the sliding mode control method to control the outer loop,
- Using the input-output method to control the inner loop,

The following text presents an introduction to the system being studied. Subsequently, two control systems are constructed for the load-side converter, to control the load voltage using nonlinear approaches. The stability of these control systems is also demonstrated. In Section 4, the performance of these structures has been evaluated by simulation in the MATLAB software coding environment. The comparison was made between the structures themselves and the linear PI technique [14] in various transient states.

2. Modeling of the system under study

This paper examines a WECS operating in off-grid mode, utilizing a SCIG as shown in Figure 3. Within this configuration, back-to-back converters operate to supply electrical power to the load through an LC filter to minimize the presence of output harmonics. The MSC and load-side converter (LSC) are interconnected via a capacitor known as the DC-link capacitor. To optimize data storage and enhance simulation speed, the average model of converters is utilized. Furthermore, this system assumes that the load's power demand is consistently lower than the wind system's power generation and that any losses incurred during the switching process are disregarded for the converters. The wind turbine is modeled using a direct current (DC) mechanical prime mover.

2.1. Squirrel-cage Induction Generator (SCIG)

The dynamic equations of the generator based on the state variables of flux and stator current in the *dq* synchronous reference frame are as follows [23]:

$$\begin{cases} \frac{d}{dt}\lambda_{sd} = V_{sd} - R_s I_{sd} + \omega_e \lambda_{sq} \\ \frac{d}{dt}\lambda_{sq} = V_{sq} - R_s I_{sq} - \omega_e \lambda_{sd} \end{cases} \quad (1)$$

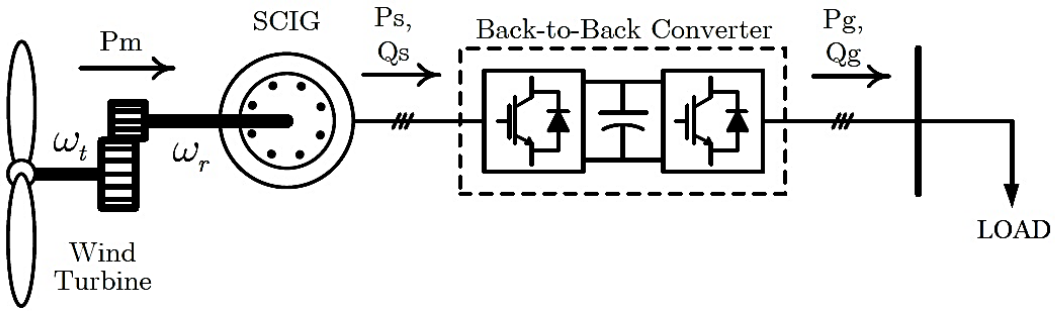

Figure 3. The schematic diagram of an off-grid WECS based on SCIG.

$$\begin{cases} \frac{d}{dt} I_{sd} = \frac{1}{\sigma L_m} \left[V_{rd} - \frac{R_r}{L_m} \left(\lambda_{sd} - L_s I_{sd} \right) + \left(\omega_e - \omega_r \right) \left(\frac{L_r}{L_m} \lambda_{sq} + L_m \sigma I_{sq} \right) \right] \\ \quad - \frac{L_r}{L_m} \left(V_{sd} - R_s I_{sd} + \omega_e \lambda_{sq} \right) \\ \frac{d}{dt} I_{sq} = \frac{1}{\sigma L_m} \left[V_{rq} - \frac{R_r}{L_m} \left(\lambda_{sq} - L_s I_{sq} \right) - \left(\omega_e - \omega_r \right) \left(\frac{L_r}{L_m} \lambda_{sd} + L_m \sigma I_{sd} \right) \right] \\ \quad - \frac{L_r}{L_m} \left(V_{sq} - R_s I_{sq} - \omega_e \lambda_{sd} \right) \end{cases} \quad (2)$$

where λ_{sdq}, V_{sdq}, I_{sdq}, and V_{rdq} are the fluxes, voltages, stator biaxial currents, and rotor biaxial voltages, respectively. Also, the ohmic resistances and inductances of the stator windings are defined as R_s, R_r, L_s, and L_r, respectively. Also, L_m is known as the mutual inductance of the rotor and stator and $\sigma = 1 - L_s L_r / L_m^2$ is the leakage factor. ω_e is the synchronous speed and ω_r is the electrical speed of the rotor, for which the dynamic equation is as follows similar to the last state variable of the machine:

$$\frac{d}{dt} \omega_r = \frac{P}{2} \frac{1}{J} \left(T_e - T_m - D \omega_r \right) \quad (3)$$

T_m, T_e, J, D and P are respectively the mechanical torque and the electromagnetic torque of the generator, the accumulated moment of inertia (including the moment of inertia of the generator and the mechanical prime mover), the accumulated damping factor, and the poles of the generator.

2.2. Load and DC Link

At the load terminal, due to the use of the RC filter, the dynamic equations of the load voltage in the biaxial *dq* synchronous frame can be written as follows in Equation (4):

$$\begin{cases} \frac{d}{dt} V_{fd} = \frac{1}{C_f} \left[I_{fd} - I_{Ldq} + \omega_e C_f V_{fq} + \xi_{vd} \right] \\ \frac{d}{dt} V_{sq} = \frac{1}{C_f} \left[I_{fq} - I_{Lq} - \omega_e C_f V_{fd} + \xi_{vq} \right] \end{cases} \quad (4)$$

In the above equations, V_{fdq}, I_{fdq}, and I_{Ldq} are the output biaxial voltage and currents of the LSC and the biaxial currents of the load connected to the system. Also, ξ_{vdq} denotes the cumulative uncertainty vectors affecting the voltage dynamics, which are caused by parametric and modeling uncertainties, and C_f is the filter capacitor. On the other hand, the following dynamic equations can be derived for the biaxial currents of the output convertera as in Equation (5):

$$\begin{cases} \frac{d}{dt} I_{fd} = \frac{1}{L_f} \left[V_{id} - R_f I_{fd} - V_{fd} + \omega_e L_f I_{fq} + \xi_{id} \right] \\ \frac{d}{dt} I_{fq} = \frac{1}{L_f} \left[V_{iq} - R_f I_{fq} - V_{fq} - \omega_e L_f I_{fd} + \xi_{iq} \right] \end{cases} \quad (5)$$

Similar to the load voltage vectors, for the biaxial currents of the LSC, ξ_{idq} are defined as uncertainty vectors. Also, R_f and L_f are the resistance and inductance of the filter. V_{idq} are the output biaxial voltages of the LSC. On the other hand, for the DC link, according to the dynamics of the capacitor C placed between the two LSC and MSC the following equation can be written as Equation (6):

$$\frac{d}{dt}V_{dc} = \frac{1}{C}(I_{dc} - I_o) \tag{6}$$

I_{dc} is the input current to the DC link through the MSC and I_o is the output current from the DC link to the LSC. If the real and reactive power of the load is represented by P_f and Q_f , we can write Equation (7) as:

$$\begin{bmatrix} P_f \\ Q_f \end{bmatrix} = \frac{3}{2}\begin{bmatrix} V_{fd} & V_{fq} \\ V_{fq} & -V_{fd} \end{bmatrix}\begin{bmatrix} I_{fd} \\ I_{fq} \end{bmatrix} \tag{7}$$

and the instantaneous active power produced by the generator ($-P_g$) can be calculated as Equation (8):

$$P_g = 1.5\left(V_{sd}I_{sd} + V_{sq}I_{sq}\right) \tag{8}$$

The currents used in Equation (6) can be calculated through the following equations:

$$\begin{cases} I_{dc} = -P_g / V_{dc} \\ I_o = P_L / V_{dc} \end{cases} \tag{9}$$

3. Design of the Control Structure

This study utilizes the control structure described in [23] for the MSC. The objective of this research is to build the control design for the LSC using two different approaches. The primary objective on the load side is to control the voltage magnitude and frequency delivered to the load. To fulfill the control objectives described above, the converter in this section should be controlled accordingly.

3.1. Load voltage controller using the first proposed method

This approach utilizes two cascade controllers. The primary objective of the first controller is to control the magnitude of the load voltage by employing the state feedback input-output technique.

$$\begin{aligned} e_{vd} &= V_{fd}^{*} - V_{fd} \\ e_{vq} &= V_{fq}^{*} - V_{fq} \end{aligned} \tag{10}$$

The synchronous dq frame on the load side is considered in such a way that the voltage vector is only in the direction of the *d* axis, and for this purpose V_{fd}^{*} is 239 V and V_{fq}^{*} is zero. In the following, the design process of a positive definite Lyapunov function is designed and defined as follows:

$$W_{V_{fdq}} = \frac{1}{2}\begin{bmatrix} e_{V_{fd}}^2 \\ e_{V_{fq}}^2 \end{bmatrix} + \frac{1}{2}\gamma_v \begin{bmatrix} \tilde{\xi}_{vd}^{\,2} \\ \tilde{\xi}_{vq}^{\,2} \end{bmatrix} \tag{11}$$

In Equation (11), γ_v is an always-positive coefficient. The difference vector of the actual value of the accumulated uncertainties affecting the voltage dynamics with their estimated value, shown by $\tilde{\xi}_{vdq}$, is calculated according to Equation (12):

$$\begin{cases} \tilde{\xi}_{vd} = \xi_{vd} - \hat{\xi}_{vd} \\ \tilde{\xi}_{vq} = \xi_{vq} - \hat{\xi}_{vq} \end{cases} \tag{12}$$

$\hat{\xi}_{vdq}$ is the estimated value of biaxial voltage uncertainties. Next, the derivative of the Lyapunov function defined in Equation (11) can be written in the following form:

$$\frac{d}{dt}W_{V_{fdq}} = \frac{d}{dt}\begin{bmatrix} V_{fd}^* \\ V_{fq}^* \end{bmatrix} - \frac{d}{dt}\begin{bmatrix} V_{fd} \\ V_{fq} \end{bmatrix} + \gamma_i \frac{d}{dt}\begin{bmatrix} \tilde{\xi}_{vd} \\ \tilde{\xi}_{vq} \end{bmatrix}\begin{bmatrix} \tilde{\xi}_{vd} \\ \tilde{\xi}_{vq} \end{bmatrix} \tag{13}$$

Considering that the derivative of the voltage reference values is zero and on the other hand $\frac{d}{dt}\tilde{\xi}_{vdq} = -\frac{d}{dt}\hat{\xi}_{vdq}$, by choosing the estimation rules according to [24] from Equation (14):

$$\frac{d}{dt}\begin{bmatrix} \hat{\xi}_{Vfd} \\ \hat{\xi}_{Vfq} \end{bmatrix} = -\frac{\sqrt{\gamma_v}}{C_f}\begin{bmatrix} e_{Vfd} \\ e_{Vfq} \end{bmatrix} \tag{14}$$

and by inserting Equation (4) into Equation (13), the control input, which is the reference currents of the LSC, can be designed as follows with a positive coefficient k_v:

$$\begin{bmatrix} I_{fd}^* \\ I_{fq}^* \end{bmatrix} = \begin{bmatrix} I_{Ld} - \omega_e C_f V_{fq} - \xi_{vd} + k_v e_{vd} \\ I_{Lq} + \omega_e C_f V_{fd} - \xi_{vq} + k_v e_{vq} \end{bmatrix} \tag{15}$$

With this control law, the derivative of the designed Lyapunov function becomes negative semi-definite, and in this way, according to Barbalat's lemma [25], the asymptotic stability of the control system of the first part can be proved. The second controller in this cascade system is supposed to be designed to control the power components and legally extract control for the reference voltage of the LSC. Having the reference currents from Equation (15), the reference values of active and reactive powers can be calculated using Equation (7):

$$\begin{bmatrix} P_f^* \\ Q_f^* \end{bmatrix} = \frac{3}{2}\begin{bmatrix} V_{fd} & V_{fq} \\ V_{fq} & -V_{fd} \end{bmatrix}\begin{bmatrix} I_{fd}^* \\ I_{fq}^* \end{bmatrix} \tag{16}$$

Now, by defining the error of the power components through Equation (17), the process of designing the control system of this section begins:

$$\begin{bmatrix} e_{P_f} \\ e_{Q_f} \end{bmatrix} = \begin{bmatrix} P_f^* \\ Q_f^* \end{bmatrix} - \begin{bmatrix} P_f \\ Q_f \end{bmatrix} \tag{17}$$

In this section, the design of the controller is done using the sliding mode method. Thus, the sliding surfaces are selected as follows:

$$\begin{bmatrix} S_P \\ S_Q \end{bmatrix} = \begin{bmatrix} e_{P_f} \\ e_{Q_f} \end{bmatrix} + k_{spq} \int_0^t \begin{bmatrix} e_{P_f} \\ e_{Q_f} \end{bmatrix} \mathrm{d}\tau \tag{18}$$

In this equation, k_{spq} is an always-positive coefficient. In the following, if the derivative of Equation (18) is taken, we have:

$$\frac{d}{dt}\begin{bmatrix} S_P \\ S_Q \end{bmatrix} = \frac{d}{dt}\begin{bmatrix} P_f^* - P_f \\ Q_f^* - Q_f \end{bmatrix} + k_{spq}\begin{bmatrix} e_{P_f} \\ e_{Q_f} \end{bmatrix} = \frac{d}{dt}\begin{bmatrix} P_f^* \\ Q_f^* \end{bmatrix} - \frac{d}{dt}\begin{bmatrix} P_f \\ Q_f \end{bmatrix} + k_{spq}\begin{bmatrix} e_{P_f} \\ e_{Q_f} \end{bmatrix} \tag{19}$$

In Equation (19), to simplify the relations of the control system, the instantaneous derivative of the reference power values is considered equal to zero. For the derivative of power components, it can be derived from Equation (7) as follows:

$$\frac{d}{dt}\begin{bmatrix} P_f \\ Q_f \end{bmatrix} = \frac{3}{2}\frac{d}{dt}\begin{bmatrix} V_{fd} & V_{fq} \\ V_{fq} & -V_{fd} \end{bmatrix}\begin{bmatrix} I_{fd} \\ I_{fq} \end{bmatrix} + \frac{3}{2}\begin{bmatrix} V_{fd} & V_{fq} \\ V_{fq} & -V_{fd} \end{bmatrix}\frac{d}{dt}\begin{bmatrix} I_{fd} \\ I_{fq} \end{bmatrix} \tag{20}$$

By placing Equations (4) and (5) in the above equation, we can write:

$$\frac{d}{dt}\begin{bmatrix} P_f \\ Q_f \end{bmatrix} = \begin{bmatrix} G_P \\ G_Q \end{bmatrix} + \begin{bmatrix} H_P \\ H_Q \end{bmatrix} + \frac{3}{2L_f}\begin{bmatrix} V_{fd} & V_{fq} \\ V_{fq} & -V_{fd} \end{bmatrix}\begin{bmatrix} V_{id} \\ V_{iq} \end{bmatrix} \tag{21}$$

where G_P, G_Q, H_P, and H_Q are defined as follows:

$$G_P = \frac{3}{2C_f}\left(\left(I_{fd} - I_{Ld} + \omega_e C_f V_{fq} + \xi_{vd}\right)I_{fd} + \left(I_{fq} - I_{Lq} - \omega_e C_f V_{fd} + \xi_{vq}\right)I_{fq}\right) \tag{22}$$

$$G_Q = \frac{3}{2C_f}\left(\left(I_{fq} - I_{Lq} - \omega_e C_f V_{fd} + \xi_{vq}\right)I_{fd} - \left(I_{fd} - I_{Ld} + \omega_e C_f V_{fq} + \xi_{vd}\right)I_{fq}\right) \tag{23}$$

$$H_P = \frac{3}{2L_f}\left(\left(-R_f I_{fd} - V_{fd} + \omega_e L_f I_{fq} + \xi_{id}\right)V_{fd} + \left(-R_f I_{fq} - V_{fq} - \omega_e L_f I_{fd} + \xi_{iq}\right)V_{fq}\right) \tag{24}$$

$$H_Q = \frac{3}{2L_f}\left(\left(-R_f I_{fd} - V_{fd} + \omega_e L_f I_{fq} + \xi_{id}\right)V_{fq} - \left(-R_f I_{fq} - V_{fq} - \omega_e L_f I_{fd} + \xi_{iq}\right)V_{fd}\right) \tag{25}$$

By inserting Equation (21) into Equation (19), the derivative of the sliding surfaces of the power components will change as follows:

$$\frac{d}{dt}\begin{bmatrix} S_P \\ S_Q \end{bmatrix} = -\begin{bmatrix} G_P \\ G_Q \end{bmatrix} - \begin{bmatrix} H_P \\ H_Q \end{bmatrix} - \frac{3}{2L_f}\begin{bmatrix} V_{fd} & V_{fq} \\ V_{fq} & -V_{fd} \end{bmatrix}\begin{bmatrix} V_{id} \\ V_{iq} \end{bmatrix} + k_{spq}\begin{bmatrix} e_{P_f} \\ e_{Q_f} \end{bmatrix} \tag{26}$$

In this way, a certain positive definite Lyapunov function is expressed as follows in the continuation of the design process:

$$W_{PQ} = \frac{1}{2}\begin{bmatrix} S_P \\ S_Q \end{bmatrix}^T \begin{bmatrix} S_P \\ S_Q \end{bmatrix} > 0 \tag{27}$$

The derivative of this function is:

$$\frac{d}{dt}W_{PQ} = \begin{bmatrix} S_P \\ S_Q \end{bmatrix}^T \frac{d}{dt}\begin{bmatrix} S_P \\ S_Q \end{bmatrix} \tag{28}$$

By inserting Equation (26) into Equation (28), the derivative of the function W_{PQ} is extracted according to Equation (29):

$$\frac{d}{dt}W_{PQ}=\begin{bmatrix}S_P\\S_Q\end{bmatrix}^T\left\{-\begin{bmatrix}G_P\\G_Q\end{bmatrix}-\begin{bmatrix}H_P\\H_Q\end{bmatrix}-\frac{3}{2L_f}\begin{bmatrix}V_{fd}&V_{fq}\\V_{fq}&-V_{fd}\end{bmatrix}\begin{bmatrix}V_{idq}\\V_{iq}\end{bmatrix}+k_{spq}\begin{bmatrix}e_{P_f}\\e_{Q_f}\end{bmatrix}\right\} \tag{29}$$

Now, to guarantee the stability of the control system, the control inputs V_{idq} are designed as the reference voltages of the LSC in such a way that the derivative of the negative semi-definite function W_{PQ} is obtained:

$$\begin{bmatrix}V_{id}^*\\V_{iq}^*\end{bmatrix}=\frac{2L_f}{3}\begin{bmatrix}V_{fd}&V_{fq}\\V_{fq}&-V_{fd}\end{bmatrix}^{-1}\left\{k_{spq}\begin{bmatrix}e_{P_f}\\e_{Q_f}\end{bmatrix}-\begin{bmatrix}G_P\\G_Q\end{bmatrix}-\begin{bmatrix}H_P\\H_Q\end{bmatrix}+k_{satpq}\begin{bmatrix}sat(S_P)\\sat(S_Q)\end{bmatrix}\right\} \tag{30}$$

k_{satpq} is also a control positive gain coefficient in Equation (30). With the above control law, the asymptotic stability of the controller can be guaranteed following Barblat's lemma, and as a result, the derivative of the designed Lyapunov function will be equal to:

$$\frac{d}{dt}W_{PQ}=-\begin{bmatrix}S_P\\S_Q\end{bmatrix}^T\left\{k_{satpq}\begin{bmatrix}sat(S_P)\\sat(S_Q)\end{bmatrix}\right\}=-k_{satpq}S_P\left\{sat(S_P)\right\}-k_{satpq}S_Q\left\{sat(S_Q)\right\}\le 0 \tag{31}$$

The voltage obtained from Equation (30) will be applied to the LSC with synchronous frequency, and thus the load frequency will be set at its nominal value.

3.2. Load voltage controller using the second proposed method

In this method, two cascade controllers are used. The first controller of this method is designed to control the size of the load voltage. Therefore, considering Equation (10), the design of the control system with the sliding mode control method is described below. For this purpose, two sliding surfaces (S_{vd} and S_{vq}) are considered as follows:

$$\begin{bmatrix}S_{vd}\\S_{vq}\end{bmatrix}=\begin{bmatrix}e_{vd}\\e_{vq}\end{bmatrix}+k_{sv}\int_0^t\begin{bmatrix}e_{vd}\\e_{vq}\end{bmatrix}\mathrm{d}\tau \tag{32}$$

where k_{sv} is a positive control gain coefficient. By Equation (32), we can write:

$$\frac{d}{dt}\begin{bmatrix}S_{vd}\\S_{vq}\end{bmatrix}=\frac{d}{dt}\begin{bmatrix}V_{fd}^*-V_{fd}\\V_{fq}^*-V_{fq}\end{bmatrix}+k_{sv}\begin{bmatrix}e_{vd}\\e_{vq}\end{bmatrix}=\frac{d}{dt}\begin{bmatrix}V_{fd}^*\\V_{fq}^*\end{bmatrix}-\frac{d}{dt}\begin{bmatrix}V_{fd}\\V_{fq}\end{bmatrix}+k_{sv}\begin{bmatrix}e_{vd}\\e_{vq}\end{bmatrix} \tag{33}$$

Considering that the derivative of voltage reference values is zero, by inserting Equation (4) into Equation (33), the derivative of sliding surfaces will be equal to:

$$\frac{d}{dt}\begin{bmatrix}S_{vd}\\S_{vq}\end{bmatrix}=-\begin{bmatrix}\left(I_{fd}-I_{Ld}+\omega_e C_f V_{fq}+\xi_{vd}\right)\\\left(I_{fq}-I_{Lq}-\omega_e C_f V_{fd}+\xi_{vq}\right)\end{bmatrix}+k_{sv}\begin{bmatrix}e_{vd}\\e_{vq}\end{bmatrix} \tag{34}$$

According to the sliding mode control method, a positive definite Lyapunov function is selected for the sliding surfaces as follows:

$$W_{Vdq}=\frac{1}{2}\begin{bmatrix}S_{vd}\\S_{vq}\end{bmatrix}^T\begin{bmatrix}S_{vd}\\S_{vq}\end{bmatrix}>0 \tag{35}$$

By taking the derivation of function W_{Vdq} and inserting Equation (34) into it:

$$\frac{d}{dt}W_{Vdq}=\begin{bmatrix}S_{vd}\\S_{vq}\end{bmatrix}^{T}\left\{-\begin{bmatrix}\left(I_{fd}-I_{Ld}+\omega_e C_f V_{fq}+\xi_{vd}\right)\\\left(I_{fq}-I_{Lq}-\omega_e C_f V_{fd}+\xi_{vq}\right)\end{bmatrix}+k_{sv}\begin{bmatrix}e_{vd}\\e_{vq}\end{bmatrix}\right\} \tag{36}$$

Now, if the biaxial reference currents of the LSC as the control input are designed as follows, the stability of the controller can be guaranteed:

$$\begin{bmatrix}I_{fd}^{*}\\I_{fq}^{*}\end{bmatrix}=\begin{bmatrix}I_{Ld}-\omega_e C_f V_{fq}-\xi_{vd}+k_{sv}e_{vd}+k_{satv}sat(S_{vd})\\I_{Lq}+\omega_e C_f V_{fd}-\xi_{vq}+k_{sv}e_{vq}+k_{satv}sat(S_{vq})\end{bmatrix} \tag{37}$$

As a result, Equation (36) will be changed as follows by inserting Equation (37) into it:

$$\frac{d}{dt}W_{Vdq}=-\begin{bmatrix}S_{vd}\\S_{vq}\end{bmatrix}^{T}\begin{bmatrix}k_{satv}sat(S_{vd})\\k_{satv}sat(S_{vq})\end{bmatrix}=-k_{satv}S_{vd}sat(S_{vd})-k_{satv}S_{vq}sat(S_{vq})\le 0 \tag{38}$$

In Equations (37) and (38), k_{satv} is the positive gain coefficient of the control. In this way, since W_{Vdq} is a positive definite function and its derivative is negative semi-definite and continuous, according to Barblat's lemma, the asymptotic stability of the designed controller can be guaranteed [25].

Now it is time to design the second controller using the IOFL method. Having the reference currents from Equation (37), the biaxial currents error of the LSC can be defined as follows:

$$\begin{bmatrix}e_{I_{fd}}\\e_{I_{fq}}\end{bmatrix}=\begin{bmatrix}I_{fd}^{*}\\I_{fq}^{*}\end{bmatrix}-\begin{bmatrix}I_{fd}\\I_{fq}\end{bmatrix} \tag{39}$$

Next, a positive definite Lyapunov function is designed:

$$W_{I_{fdq}}=\frac{1}{2}\begin{bmatrix}e_{I_{fd}}^{2}\\e_{I_{fq}}^{2}\end{bmatrix}+\frac{1}{2}\gamma_i\begin{bmatrix}\tilde{\xi}_{id}^{2}\\\tilde{\xi}_{iq}^{2}\end{bmatrix} \tag{40}$$

In the above equation, γ_i is a positive number and $\tilde{\xi}_{idq}$ shows the difference between the actual value (ξ_{idq}) of the accumulated uncertainty vectors affecting the flow dynamics and their estimated value ($\hat{\xi}_{idq}$):

$$\tilde{\xi}_{idq}=\xi_{idq}-\hat{\xi}_{idq} \tag{41}$$

In this way, the derivative of Equation (40) can be written as follows:

$$\frac{d}{dt}W_{I_{fdq}}=\frac{d}{dt}\begin{bmatrix}I_{fd}^{*}\\I_{fq}^{*}\end{bmatrix}-\frac{d}{dt}\begin{bmatrix}I_{fd}\\I_{fq}\end{bmatrix}+\gamma_i\frac{d}{dt}\begin{bmatrix}\tilde{\xi}_{id}\\\tilde{\xi}_{iq}\end{bmatrix}\begin{bmatrix}\tilde{\xi}_{id}\\\tilde{\xi}_{iq}\end{bmatrix} \tag{42}$$

Table 1. Values of studied system parameters and control coefficients.

Rated power of the machine and converters (P_n)	746 W	DC-link voltage	400 v	k_{sv}	0.245
Rated voltage of the system (V_n)	415 V	DC-link capacitor (C)	1650 µF	k_{satv}	0.05
Stator resistance (R_s)	9.919 Ω	Filter resistance (R_f)	0.25 Ω	k_{spq}	1000
Rotor resistance (R_r)	4.628 Ω	Filter inductance (L_f)	0.006 H	k_{satpq}	5
Stator inductance (L_s)	0.9291 H	Filter capacitance (C_f)	41 µF	k_v	0.245
Rotor inductance (L_r)	0.9291 H	Resistive load	173 W	k_i	180
Magnetizing inductance (L_m)	0.8895 H	Resistive-inductive load	70W+546 VAR	γ_v	1.681×10^{-7}
Number of poles (P)	4	Inertia moment (J)	0.0525 kg.m^2	γ_i	0.0036

Considering that $\frac{d}{dt}\tilde{\xi}_{idq} = -\frac{d}{dt}\hat{\xi}_{idq}$ and choosing the estimation rule from the following equations [24]:

$$\frac{d}{dt}\begin{bmatrix}\hat{\xi}_{Ifd}\\ \hat{\xi}_{Ifq}\end{bmatrix} = -\frac{\sqrt{\gamma_i}}{L_f}\begin{bmatrix}e_{Ifd}\\ e_{Ifq}\end{bmatrix} \tag{43}$$

If the reference voltages of the LSC (V_{idq}) are designed as the control input of the second controller to control the output currents of the LSC, as follows:

$$\begin{bmatrix}V_{id}^*\\ V_{iq}^*\end{bmatrix} = R_f\begin{bmatrix}I_{fd}\\ I_{fq}\end{bmatrix} + \begin{bmatrix}V_{fd}\\ V_{fq}\end{bmatrix} + \omega L_f\begin{bmatrix}-I_{fq}\\ I_{fd}\end{bmatrix} + L_f\frac{d}{dt}\begin{bmatrix}I_{fd}^*\\ I_{fq}^*\end{bmatrix} + k_i\begin{bmatrix}e_{Ifd}\\ e_{Ifq}\end{bmatrix} - \begin{bmatrix}\hat{\xi}_{Ifd}\\ \hat{\xi}_{Ifq}\end{bmatrix} \tag{44}$$

and are placed in Equation (42) together with Equation (43), it can be shown that $\frac{d}{dt}W_{I_{fdq}} \le 0$ and, according to Barbalat's lemma [23], the asymptotic stability of the controller is guaranteed. It should be noted that in the above control law, k_i is a positive control coefficient.

As in the previous part, the voltage obtained from Equation (44) will be applied to the LSC with the synchronous frequency, and in this way, the load frequency will be set at the desired nominal value.

4. Simulation and analysis of results

In this section, the initial settings of system parameters are presented based on Table 1. The specified parameters are selected from [14]. Given that the control system structures designed in the previous section are nonlinear, three disturbances have been taken into account to assess the robustness of these structures.

These disturbances include uncertainty in the system parameter, change in the operating point of the system, and a disturbance with a large amplitude, each is

individually scrutinized. However, to assess the effectiveness of proposed method 1 and proposed method 2, the simulation results were compared with each other and with the results of the traditional PI linear control system mentioned in [14]. In simulation results, the term "Proposed" refers to the proposed control structure 2, "PI" refers to the PI control structure [14], and "SMC-PQ" refers to the proposed structure 1.

The simulations were conducted using the MATLAB software coding environment on a personal computer equipped with an Intel® Core™i7 processor operating at a frequency of 2.5GHz. The computer had 8 GB of RAM and ran on a 64-bit operating system version 10.

4.1. Parametric uncertainty

At the 0.5 s mark, a 10% rise is regarded as an uncertainty in the stator resistance. It is important to mention that this uncertainty is just applicable to the system model. Figure 4 (a) depicts the load voltage changes graph, which demonstrates that all three approaches exhibited robust behavior. However, the proposed method 2 displayed far fewer transient states and returned to its previous value at a faster rate. Furthermore, as depicted in this diagram, the power components are determined by the multiplication of the output voltage and current of the LSC. Consequently, any changes in the voltage directly impact the performance of the internal power control loop. As a result, the fluctuations observed in the proposed method 1 are more pronounced compared to the other two methods.

Figures 4(b) and (c) depict the variations in the active and reactive output power of the LSC. The uncertainty in the parameter has resulted in a temporary change in the output power components of the grid-side converter. Although the transitory state of the findings from proposed method 2 is not particularly important, the results from PI techniques and proposed method 1 have returned to their prior value after a transient state. Figure 4(d) illustrates the variations in the DC-link voltage. The introduction of parameter uncertainty does not have a substantial impact on the output active power.

The voltage quickly returns to its initial value after a satisfactory transient state in all three methods. However, the results from proposed method 2 demonstrate a faster convergence rate. Figures 4(e) and (f) display the flux and torque of the machine, respectively. The results obtained from nonlinear methods 1 and 2 are indistinguishable, whereas the PI method exhibits a distinct transient state.

The findings from Figures 4(a) to (f) validate that the proposed method 2, apart from its robustness against parameter uncertainties, exhibits superior efficiency compared to both the linear PI technique and the proposed method 1.

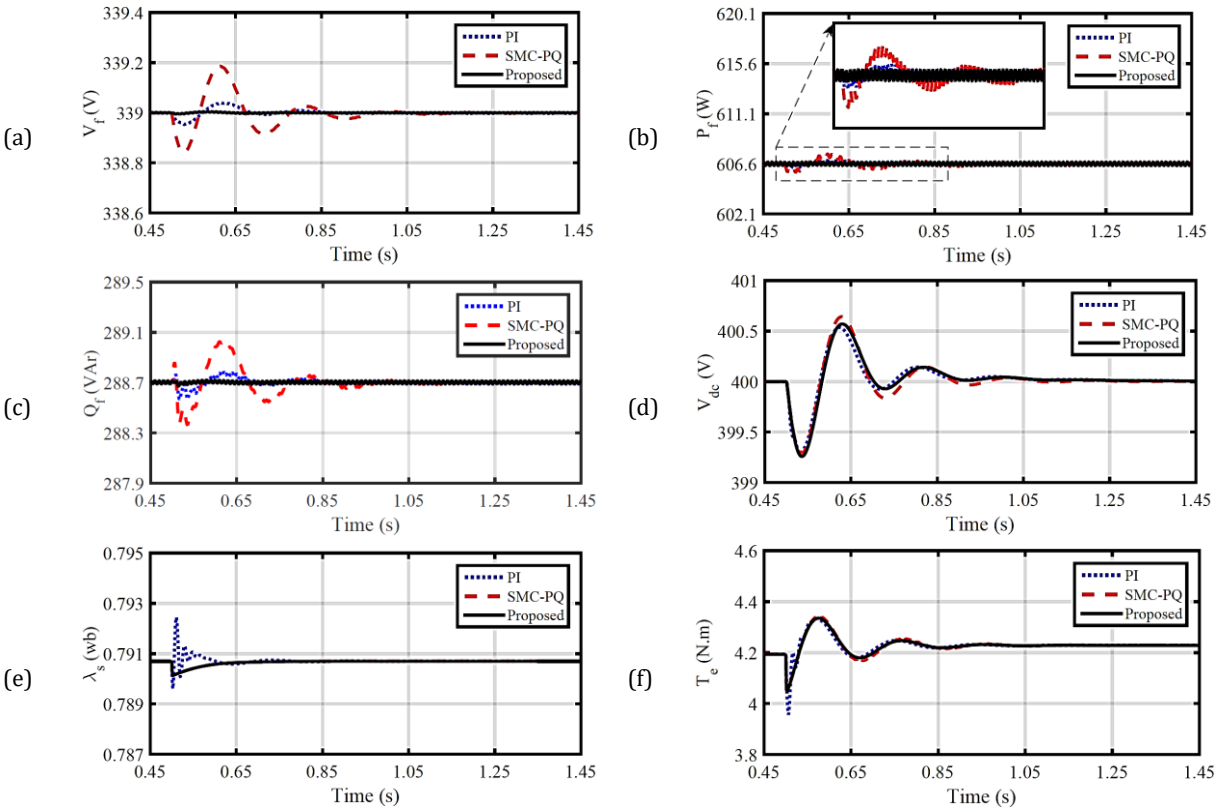

Figure 4. Simulation results when applying parametric uncertainty, respectively, for load terminal voltage, active power injected into the load, load reactive power, DC-link voltage, stator flux and electromagnetic torque of the machine for three control structures.

4.2. Changing the system's operating point

In this scenario, the impedance of the balanced resistive load increases by 5% from the moment of 1.5 s. Figure 5 shows the behavior of important system parameters on the load side and the machine side. Figure 5(a) demonstrates that the load voltage in proposed method 2 exhibits a reduced transient state and a greater convergence speed.

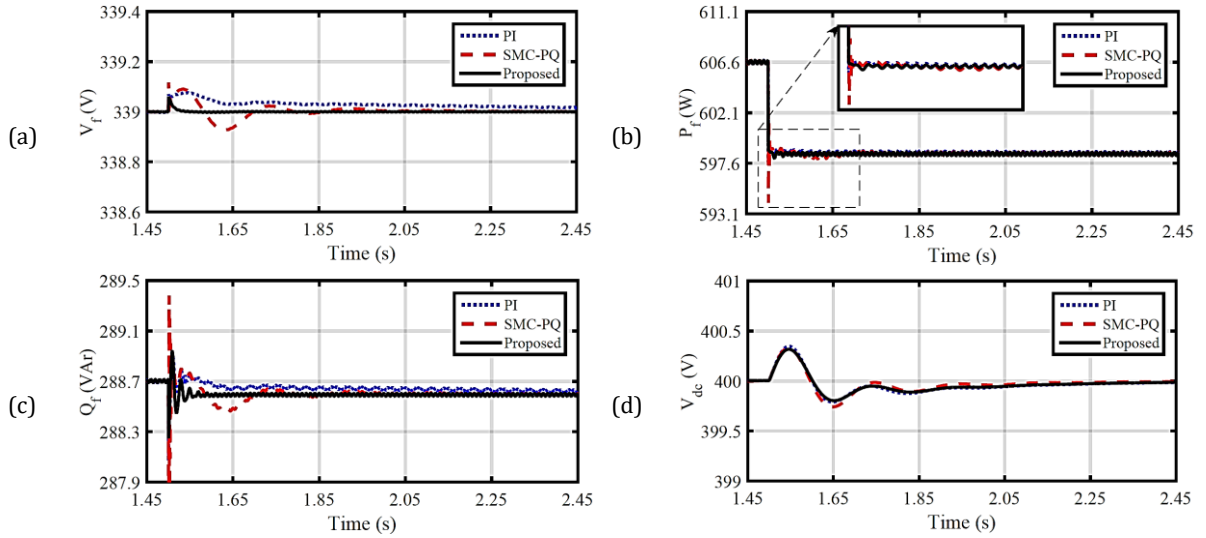

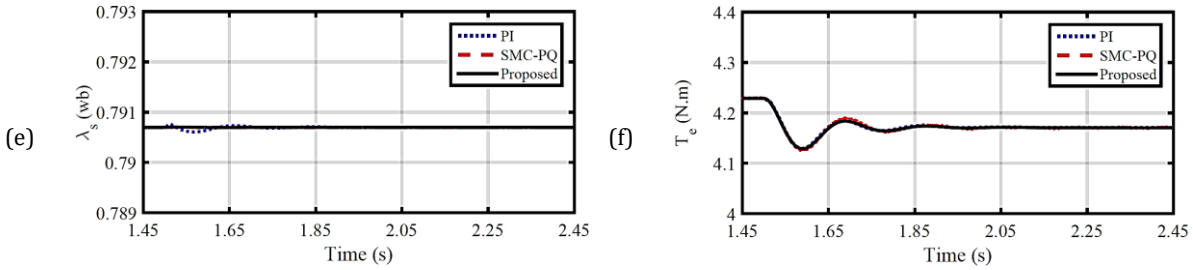

Figure 5. Simulation results when changing the operating point of the system, respectively, for the load terminal voltage, active power injected into the load, load reactive power, DC-link voltage, stator flux and electromagnetic torque of the machine for three control structures.

Furthermore, due to its suitability for adjustment rather than tracking, the PI technique has not yet reached its final value within the range of the given shape. While the suggested control method 1 shows a faster convergence speed compared to the PI technique, its transient state is more severe than that of proposed method 2. Figures 5(b) and (c) depict the variations in the active and reactive powers of the LSC. It is evident that in all three approaches, the power components reach their new reference values after a temporary period. However, the suggested method 2 demonstrates superior speed and transient state performance compared to the other techniques. Figure 5(d) displays the variations in the DC-link voltage. The outcomes of all three approaches are nearly identical to one another. Nevertheless, approach 2 has superior transitivity. Figures 5(e) and (f) additionally illustrate the alterations in the flux and torque of the machine. It is evident that there have been no substantial fluctuations in the machine flux, and the outcomes of both suggested nonlinear approaches are in agreement with each other. The torque of the machine is decreased in all three approaches to restore the equilibrium between power production and consumption in response to load variations.

4.3. Large disturbance

In this section, at the moment of 2.5 s, the total impedance of the load reaches 30% of its nominal value and returns to its normal state after half a power cycle (0.01 s). This situation can be considered similar to a symmetrical three-phase short circuit at the load terminal.

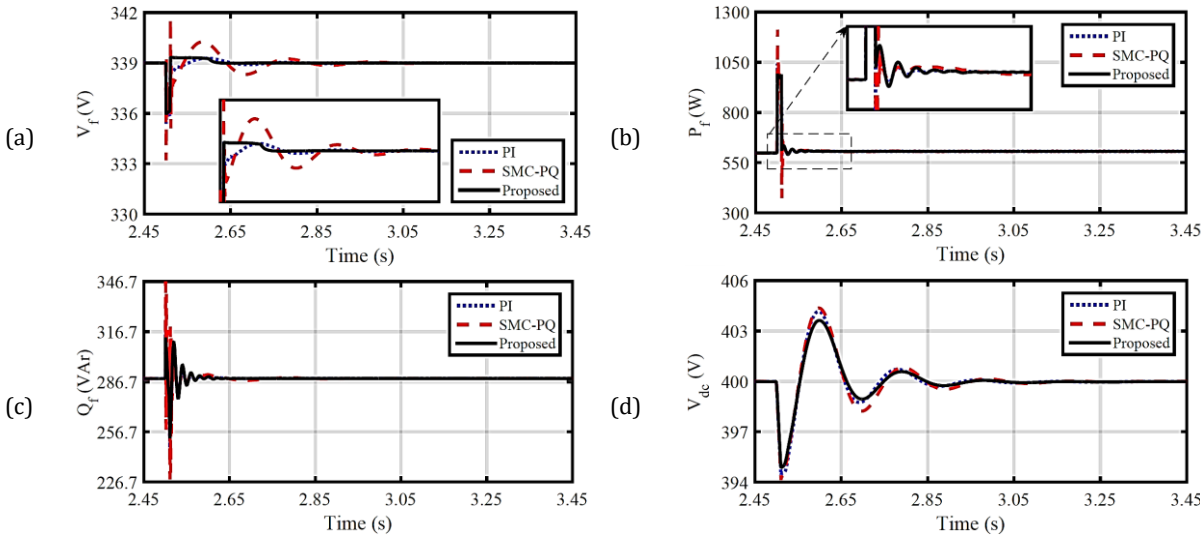

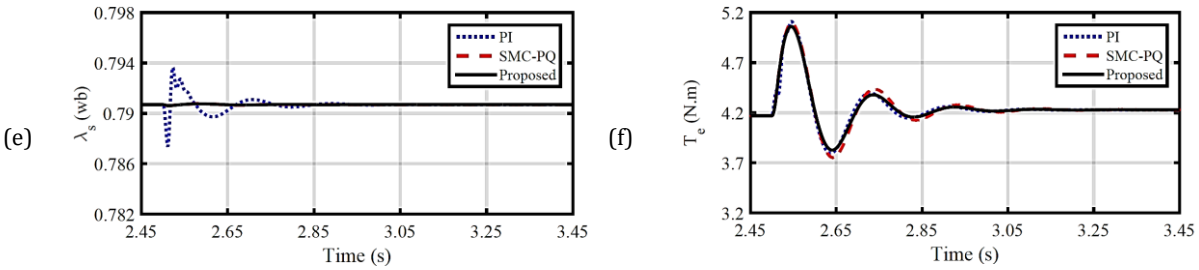

Figure 6. Simulation results during large disturbances in the system for load terminal voltage, active power injected to load, load reactive power, DC-link voltage, stator flux and machine electromagnetic torque for three control structures.

Figure 6(a) illustrates the variations in load voltage following the application of short circuit conditions. Despite experiencing a significant decrease during short circuits, all three methods exhibit this behavior. However, in proposed method 2, the load voltage reaches its nominal value more efficiently and rapidly, displaying a more appropriate transient state and speed. Figures 6(b) to (d) depict the output power components of the LSC and the DC-link voltage, respectively. These figures illustrate that the occurrence of short-circuit circumstances has resulted in a significant transient state in all three ways. However, the proposed technique 2 has achieved faster convergence of the indicated variables to their previous levels. Figures 6(e) and (f) display the flux and torque of the machine. There are no substantial alterations in the flux of the machine in proposed techniques 1 and 2. The machine's torque has returned to its original value after a transient state in all three techniques. However, the proposed method 2 exhibits a faster rate of convergence compared to the other two methods.

5. Conclusion

This work presents two nonlinear robust control architectures for the LSC of a SCIG-based WECS operating in off-grid mode. A comparison has been made between the simulation results of the two suggested systems and the PI technique under three common disturbances: parametric uncertainty, system operating point change, and major disturbance. Both proposed structures exhibit superior suitability and resilience compared to the PI technique. However, the performance of control structure 2 demonstrates a more favorable reaction in transient states induced by disturbances, in contrast to method 1. The cause for this can be elucidated as follows: in suggested method 1, voltage and current variations manifest concurrently in the control structure predicated on power components, but in proposed method 2, these fluctuations manifest solely in each control loop individually. In summary, the obtained results are as follows:

- Designing and implementing a hybrid control method to control SCIG-based WECS operating in off-grid mode.
- Optimal and flexible control to balance and stabilize the load voltage.

References

[1] A. Gatto, "The Energy Futures We Want: A Research and Policy Agenda for Energy Transitions," *Energy Research & Social Science*, vol. 89, 102639, 2022.

[2] S. Frank, H. Böttcher, et al., "Dynamics of the Land Use, Land Use Change, and Forestry Sink in the European Union: The Impacts of Energy and Climate Targets for 2030," *Climatic Change*, vol. 138, pp. 253-266, 2016.

[3] C. Vázquez-Hernández, J. Serrano-González, and G. Centeno, "A Market-Based Analysis on the Main Characteristics of Gearboxes Used in Onshore Wind Turbines," *Energies*, vol. 10, no. 11, p. 1686, 2017.

[4] M. M. Ahmed, W. S. Hassanein, and M. A. Enany, "Proposing and Evaluation of SC Techniques for Variable Speed High-Power Operation of SEIG," *IEEE Access*, vol. 8, pp. 20666-20675, 2020.

[5] M. Shiraliyan, P. Sharma, and C. Sharma, "Automatic Reactive Power Control of Isolated Wind–Diesel Hybrid Power System using Artificial Bee Colony and Gray Wolf Optimization," *International Journal of Green Energy*, vol. 15, no. 14-15, p. 889-904, 2018.

[6] T. Telsnig, A. Georgakaki, et al., "Clean Energy Technology Observatory: Wind Energy in the European Union–2022 Status Report on Technology Development, " *Trends, Value Chains and Markets*, 2022.

[7] M. M. Rezaei, "A Nonlinear Maximum Power Point Tracking Technique for DFIG-Based Wind Energy Conversion Systems," *Engineering science and technology, an international journal*, vol. 21, no. 5, pp. 901-908, 2018.

[8] A. Sotoudeh, J. Soltani, and M. M. Rezaei, "A Robust Control for SCIG-Based Wind Energy Conversion Systems Based on Nonlinear Control Methods," *Journal of Control, Automation and Electrical Systems*, vol. 32, pp. 735-746, 2021.

[9] S. K. Tiwari, B. Singh, and P. K. Goel, "Design and Control of Microgrid Fed by Renewable Energy Generating Sources," *IEEE Transactions on Industry Applications*, vol. 54, no. 3, pp. 2041-2050, 2018.

[10] M. El Achkar, R. Mbayed, G. Salloum, N. Patin, and E. Monmasson, "Voltage Control of a Stand-Alone Cascaded Doubly Fed Induction Generator," *IEEE Transactions on Industrial Electronics*, vol. 66, no. 1, pp. 762-771, 2018.

[11] R. Mishra, and T. K. Saha, "Control of SCIG Based Constant Voltage Generation Scheme for Distributed Power Supply," *International Journal on Electrical Engineering and Informatics*, vol. 10, no. 3, pp. 513-525, 2018.

[12] R. Mishra, and T. K. Saha, "Control of A Stand-Alone Distributed Generation System with Unbalanced and Nonlinear Load," *International Transactions on Electrical Energy Systems*, vol. 30, no. 4, pp. e12286, 2020.

[13] M. Abdelrahem, C. M. Hackl, R. Kennel, and J. Rodriguez, "Efficient Direct-Model Predictive Control with Discrete-Time Integral Action for PMSGs," *IEEE Transactions on Energy Conversion*, vol. 34, no. 2, pp. 1063-1072, 2019.

[14] R. Mishra, and T. K. Saha, "Combined Control of Stand-Alone Energy Conversion Scheme for Distributed Sources: Development and Performance Analysis," *International Journal of Electrical Power & Energy Systems*, vol. 115, 105480, 2020.

[15] R. Mishra, and T. K. Saha, "Modelling and Analysis of Distributed Power Generation Schemes Supplying Unbalanced and Nonlinear Load," *International Journal of Electrical Power & Energy Systems*, vol. 119, 105878, 2020.

[16] A. Sotoudeh, and M. M. Rezaei, "Robust Control of Isolated SCIG-Based WECS Feeding Constant Power Load using Adaptive Backstepping and Fractional Order PI Methods," *International Journal of Dynamics and Control*, vol. 12, no. 2, pp. 452-462, 2024.

[17] L. Xiong, P. Li, and J. Wang, "High-Order Sliding Mode Control of DFIG under Unbalanced Grid Voltage Conditions," *International Journal of Electrical Power & Energy Systems*, vol. 117, 105608, 2020.

[18] S. Huang, J. Wang, et al., "A Fixed-Time Fractional-Order Sliding Mode Control Strategy for Power Quality Enhancement of PMSG Wind Turbine," *International Journal of Electrical Power & Energy Systems*, *vol.* 134, 107354, 2021.

[19] H. H. Mousa, A. R. Youssef, and E. E. Mohamed, "Optimal Power Extraction Control Schemes for Five-Phase PMSG Based Wind Generation Systems," *Engineering science and technology, an international journal*, vol. 23, no. 1, pp. 144-155, 2020.

[20] Z. Jai Andaloussi, A. Raihani, A. El Magri, R. Lajouad, and A. El Fadili, "Novel Nonlinear Control and Optimization Strategies for Hybrid Renewable Energy Conversion System," *Modelling and simulation in engineering*, vol. 2021, no. 1, p. 3519490, 2021.

[21] J. Ebrahimi, and M. Abasi, "Design of a Power Management Strategy in Smart Distribution Networks with Wind Turbines and EV Charging Stations to Reduce Loss, Improve Voltage Profile, and Increase Hosting Capacity of the Network," *Journal of Green Energy Research and Innovation*, vol. 1, no. 1, pp. 1-15, 2024.

[22] A. A. Karimi Taleb, H. Makvandi, and A. Oraee , "The Impact of Wind Direction on Wind Farms' Output Power and Income," *Journal of Green Energy Research and Innovation*, vol. 1, no. 1, pp. 34-47, 2024.

[23] A. Sotoudeh, and M. M. Rezaei, "An Adaptive Control Strategy for Grid-Forming of SCIG-Based Wind Energy Conversion Systems," *Energy Reports*, vol. 10, pp. 114-122, 2023.

[24] M. M. Rezaei, and J. Soltani, "A Robust Control Strategy for a Grid-Connected Multi-Bus Microgrid under Unbalanced Load Conditions," *International Journal of Electrical Power & Energy Systems*, vol. 71, pp. 68-76, 2015.

[25] M. Abasi, M. Falah Nezhadnaeini, M. Karimi, and N. Yousefi "A Novel Meta heuristic Approach to Solve Unit Commitment Problem in The Presence of wind Farms" *Revue roumaine des sciences techniques Serie Electrotechnique et Energetique*, vol. 60, no. 3, pp. 253–262, 2015.

Declaration of Competing Interest

The authors declare that they have no known competing financial interests or personal relationships that could have appeared to influence the work reported in this paper. The ethical issues, including plagiarism, informed consent, misconduct, data fabrication and/or falsification, double publication and/or submission, redundancy, have been completely observed by the authors.

Credit Authorship Contribution Statement

Adel Sotoudeh: Conceptualization, Data curation, Formal analysis, Investigation, Roles/Writing - original draft, Writing-review & editing. **Mohammad Mahdi Rezaei:** Methodology, Project administration, Writing-review & editing. **Mohammadreza Moradian:** Methodology, Validation, Visualization, Roles/Writing-original draft, Writing-review & editing.

Bibliography

Adel Sotoudeh was born in Iran in 1989. He received his Ph.D. degree in Electrical Engineering (Power system) from Khomeinishahr Branch, Islamic Azad University, Khomeinishahr /Isfahan, Iran, in 2023. Also, he has taught for ten years at Khorasgan Islamic Azad University and sama college. He has published 4 research papers. His research interests include power quality, smart grids, design, optimization and implementation of electrical drives, and microgrids.

Mohammad Mahdi Rezaei received the M.Sc. degree in electrical engineering from Amirkabir University of Technology (Tehran Polytechnic), Tehran, Iran, in 2007, and the Ph.D. degree in electrical engineering from the Science and Research Branch, Islamic Azad University, Tehran, Iran, in 2015. He is currently an Associated Professor in the Department of Electrical and Computer Engineering, Khomeinishahr Branch, Islamic Azad University, Isfahan, Iran. His main areas of research are control of microgrids, distributed generations, and design, optimization and implementation of electrical drives.

Mohammadreza Moradian received the M.Sc. degree in electrical engineering from Isfahan University of Technology, Isfahan, Iran, in 2001, and the Ph.D. degree in electrical engineering from the Science and Research Branch, Islamic Azad University, Tehran, Iran, in 2016. He is currently an Associated Professor in the Department of Electrical and Computer Engineering, Najafabad Branch, Islamic Azad University, Isfahan, Iran. His main areas of research are electrical machines and drives, distributed generations, and design, power system reliability.